Analytical Chemistry, Volume 94, Issue 39, October 2022, pp. 13598-13606
DOI:10.1021/acs.analchem.2c03387

Ultrathin Graphdiyne/Graphene Heterostructure as a Robust Electrochemical Sensing Platform

Xiuchao Sun[a], Menglu Duan[a], Rongteng Li[a], Yuan Meng[a], Qiang Bai[a], Lina Wang[b,*], Manhong Liu[a], Zhugen Yang[c], Zhiling Zhu[a,*], Ning Sui[a,*]

[a] *College of Materials Science and Engineering, Qingdao University of Science and Technology, Qingdao, Shandong 266042, China*

[b] *College of Environment and Safety Engineering, Qingdao University of Science and Technology, Qingdao 266042, China*

[c] *School of Water, Energy and Environment, Cranfield University, Milton Keynes, MK43 0AL, United Kingdom*

** Corresponding authors: linawang@qust.edu.cn (L. Wang), zlzhu@qust.edu.cn (Z. Zhu), suining@qust.edu.cn (N. Sui)*

ABSTRACT: Graphdiyne (GDY) has been considered as an appealing electrode material for electrochemical sensing since its alkyne-rich structure and high degrees of π-conjugation, which shows great affinity to heavy metal ions and pollutant molecules via d–π and π–π interactions. However, the low surface area and poor conductivity of bulk GDY limit its electrochemical performance. Herein, two dimensional ultrathin graphdiyne/graphene (GDY/G) nanostructure was synthesized and used as electrode materials for electrochemical sensing. Graphene plays the roles of an epitaxy template for few-layered GDY growth and conductive layer. The formed few-layered GDY with high surface area possesses abundant affinity sites toward heavy metal ions (Cd^{2+}, Pb^{2+}), toxic molecules, e.g., nitrobenzene (NB), 4-nitrophenol (4-NP), via d–π and π–π interactions, respectively. Moreover, hemin as a key part of enzyme catalytic motif was immobilized on GDY/G via π–π interaction. The artificial enzyme mimic hemin/GDY/G modified electrode exhibited promising ascorbic acid (AA) and uric acid (UA) detection performance with excellent sensitivity and selectivity, good linear range and reproducibility. More importantly, real sample detection and the feasibility of this electrochemical sensor as a wearable biosensor were demonstrated.

Published by ACS. This is the Author Accepted Manuscript issued with: Creative Commons Attribution Non-Commercial License (CC:BY:NC 4.0).
The final published version (version of record) is available online at DOI:10.1021/acs.analchem.2c03387. Please refer to any applicable publisher terms of use.

1. INTRODUCTION

Due to the high sensitivity, fast response time, and wide detection range of electrochemical sensor, it has been widely used in the fields of disease detection,[1-3] environmental monitoring,[4, 5] drug screening,[6, 7] etc. The electrode material is an important role for electrochemical sensor, as it can affect the detection in the aspects of the rate of heterogeneous electron transfer (e.g., response time), the double layer capacitance (e.g., limit of detection), the nature of the coupling chemistry. The electrode material plays the role of selectively interacting with the analyte and converting the result into electrochemical signals, thus, electrode material with high selectivity and high conductivity is the preferred material for electrochemical sensor. To pursue a high sensitivity, nanomaterial is regarded as a promising electrode material, because it has high surface area, which can increase the active electrode area since the faradaic current depends directly on the active area of electrode. Nowadays, many electrode materials have been developed including noble metal nanostructures,[8] carbon materials,[9] and metal oxide nanostructures,[10] etc. Although noble metal nanostructure is regarded as high activity electrode material in electrochemical sensing, it has the disadvantages of poor stability, high cost and complex preparation process, which restrict its application. The poor conductivity of metal oxide nanostructure has become an obstacle in its application as electrode material, material with high conductivity is always combined to improve the conductivity of electrode, such as graphene. Thi et al. loaded Fe_3O_4 onto graphene and increased the response current by a factor of 20.[11] Carbon nanostructure shows high stability, low cost, excellent conductivity, and facile surface functionalization, is regarded as a promising electrode material for electrochemical sensor, such as graphene,[12] carbon nanotube,[13] active carbon,[14] and graphdiyne,[15] etc.

GDY is a new member of carbon allotropes with two dimensional (2D) layers characteristic. Each hexagonal benzene ring is bridged by six alkynyl linkages (-C≡C-C≡C-) and the carbon atoms are hybridized in forms of sp and sp^2. The unique structure endows GDY with fascinating properties, such as highly conjugated π electronic structures, abundant chemical bonds, highly carrier mobility and stability.[16] Plenty of well-defined GDY nanostructures including 0D nanoparticles,[17] 1D nanowires,[18] 2D nanosheets,[19] and 3D structures were reported.[20] These GDY structures were used as electrode materials in versatile electrochemical sensing. Li et al. reported a GDY powder modified electrode presents high sensitivity for metal ions detection,[21] due to the high affinity between metal ions and alkynyl bonds. Niu et al. reported a nitrogen doped GDY powder as electrode material for detection environment pollutants,[22] the

doping N atoms can enhance the electrical conductivity, which improved its electrochemical sensing performance. 2D nanostructures attract tremendous attention because of their anisotropic morphology greatly expanded surface area with the exposure of more active sites, endowing the electrode exhibits ultra-high surface sensitivity to the environment. The development of few-layered GDY 2D nanostructure is expected to improve its electrochemical activity. However, few electrochemical sensors were reported based on few-layered GDY as the electrode material since the synthesis of such few-layered GDY remains challenging.

In this study, few-layered GDY was synthesized by using liquid-exfoliated graphene as an epitaxy template. Moreover, the presence of graphene significantly enhances the conductivity of GDY/G heterostructure, which can improve the performance of electrochemical sensing. GDY shows great affinity to metal ions (via d–π conjugation due to the presence of C≡C) and molecule consisting of π electronic structure (via π-π attraction due to highly conjugated π electronic structures of GDY). GDY/G modified electrode was demonstrated as an efficient electrochemical sensor, it shows high sensitivity for heavy metal ions (Cd^{2+}, Pb^{2+}) and toxic molecules (NB, 4-NP) detection. Hemin as a key part of enzyme catalytic motif was immobilized on GDY/G via π-π interaction. Its electrochemical sensing performance is enhanced by using GDY/G as support. Hemin/GDY/G was successfully used for AA and UA detection. In all, GDY/G is evidenced to be an efficient electrode material to improve the electrochemical sensing, which holds a wide spectrum of applications in environmental monitoring and biomedical diagnosis.

2. EXPERIMENTS

2.1. Chemicals and materials

Cadmium nitrate tetrahydrate ($Cd(NO_3)_2 \cdot 4H_2O$, 99%), lead(II) nitrate ($Pb(NO_3)_2$, ≥99%), 4-NP (≥99%), NB (≥99.7%) purchased from Aladdin Chemical Reagent Co., Ltd. AA (≥99.7%) was purchased from Sinopharm Chemical Reagent Co., Ltd. UA (98%) was purchased from Shanghai Macklin Biochemical Co. Ltd. (Shanghai, China). All chemicals were not further purified before use. All ultrapure water (18.25 MΩ·cm) was prepared by a Milli-Q system (USA).

2.2. Synthesis of GDY/G

GDY/G was synthesized from our previously work.[23] Tetrabutylammonium fluoride (TBAF) (1 M in THF, 1 mL) was added into a solution of 100 mg hexakis[(trimethylsilyl)-ethynyl]benzene (HEB-TMS) and 40 mL dichloromethane (DCM) and stirred at 0 °C for 15 min. Then, the mixture was washed with deionized water, dried by anhydrous $MgSO_4$, and filtered. The precursor HEB was added dropwise into a three-necked flask containing a 40 mL pyridine solution of mixed 10 mg graphene and 50 mg $Cu(OAc)_2$. The mixture was then kept at room temperature in the dark under argon atmosphere for 1 day. The solid product was collected by centrifugation and washed with pyridine, DMF, 1 M HCl and ultrapure water. Finally, the precipitate was freeze-drying to obtain the final product GDY/G.

2.3. Preparation of the modified electrode

Before the modification, the glassy carbon electrode (GCE) of 3 mm diameter was cleaned by polish with 0.3 and 0.05 μm alumina slurries and then rinsed with ethanol and ultrapure water to get a fresh surface to use. 5 mg GDY/G was dispersed into 1 mL equal volume ultrapure water, ethanol, and 0.5 wt % nafion solution, and it was uniformly dispersed after ultrasonic treatment. Then 5 μL of homogeneous solution was dropped on the GCE surface, and dried in the air to get the GDY/G modified electrode.

2.4. Electrochemical measurements

Electrochemical determination was carried out with CHI-660E electrochemical workstation (Shanghai Chenhua Instruments Limited, China). A standard three-electrode cell was used for the electrochemical experiments. Ag/AgCl (3 M KCl) electrode, modified GCE, and platinum wire electrode were used as the reference, working, and counter electrode, respectively. According to the definition of International Union of Pure and Applied Chemistry (IUPAC), the estimation formula of the limit of detection (LOD) is:

$$LOD = K \times S_b / m \quad (1)$$

Where S_b is the standard deviation (SD) of the reaction of blank solution (without analyte); m is the slope of the analyte in the linear detection range; and K is a numerical factor selected based on the expected confidence level (K=3 is used, allowing a confidence level of 99.86%).

3. RESULTS AND DISCUSSION

3.1. Morphological and structural characterization

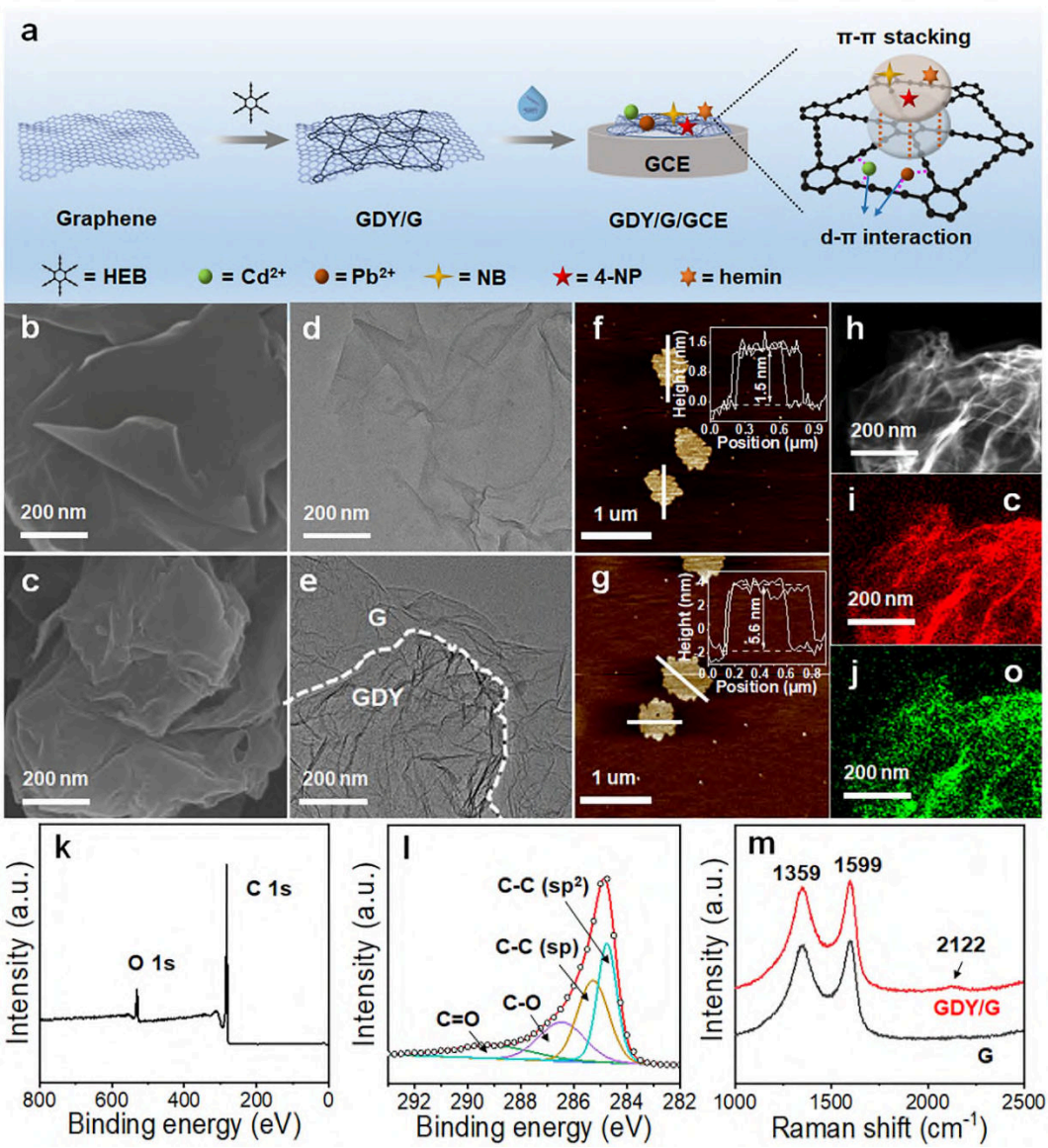


Fig. 1. (a) Schematic illustration of the preparation of GDY/G heterostructure and its application in the detection of heavy metal ions (Cd^{2+}, Pb^{2+}) and toxic molecules (NB, 4-NP). (b~g) SEM, TEM, and AFM images of (b, d, f) graphene and (c, e, g) GDY/G. (h~j) STEM image and EDS elemental maps of GDY/G for (i) C and (j) O elements. (k) XPS survey spectra of GDY/G. (l) XPS C 1s spectrum of GDY/G. (m) Raman shift of graphene and GDY/G.

Fig. 1a illustrates the preparation process of the GDY/G heterostructure. Ultrathin GDY/G heterostructure was constructed using graphene as structure guiding template. Due to lattice match and the van der Waals interaction between GDY and graphene, GDY film was easy to grow on the surface of graphene.[24, 25] The morphology of the product was analyzed by scanning electron microscope (SEM) (**Figs. 1b, 1c**). Compared with pristine graphene, the surface of graphene is rough after GDY growth. Transmission electron microscopy (TEM) image confirms that GDY/G is a lamellar structure, consistent with the morphology of graphene sheets, indicating that GDY grows in planes on graphene (**Figs. 1d, 1e**). In comparison, GDY was prepared in the same way but without graphene as a template, a 3D amorphous structure was obtained (**Fig. S1**). Atomic force microscopy (AFM) shows that graphene and GDY/G has thin thickness of 1.5 nm and 5.6 nm, respectively (**Figs. 1f, 1g**). In **Figs. 1h~k**, energy-dispersive spectroscopy (EDS) elemental mapping and X-ray photoelectron spectroscopy (XPS) images imply that GDY/G consisted mainly of carbon, which is uniformly distributed throughout the film. The presence of oxygen may be due to adsorption of oxygen from the air or unavoidable defects.[26] The C 1s spectrum that can be deconvoluted into four peaks belonging to the C=C, C≡C, C−O, and C=O bonds (**Fig. 1l**), respectively.[25] **Fig. 1m** is the Raman spectra of graphene and GDY/G. In the Raman spectra of graphene, the peaks located at 1348 and 1601 cm^{-1} correspond to the D and G bands.[23, 27] In the Raman spectra of GDY/G, the peaks located at 1359 cm^{-1} and 1599 cm^{-1} are graphene lattice vibrations, and 2122 cm^{-1} can be attributed to the C≡C bond vibrations of GDY.[23, 28]

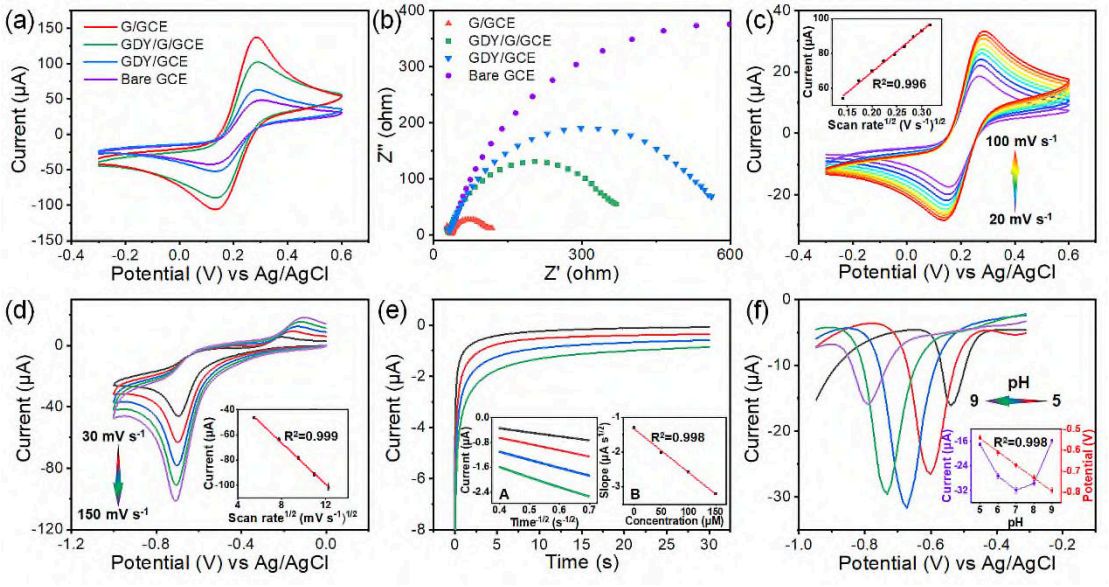


Fig. 2. (a) CV curves and (b) Electrochemical impedance spectroscopy of Bare GCE, G/GCE, GDY/GCE, and GDY/G/GCE in 5.0 mM $[Fe(CN)_6]^{3-/4-}$ solution containing 0.1 M KCl. (c) CV curves of GDY/G/GCE in 5.0 mM $[Fe(CN)_6]^{3-/4-}$ solution containing 0.1 M KCl at different scan rates. Inset: the linear relationship between the anodic peak currents and the square root of scan rate. (d) CV curves obtained at different scan rates for the GDY/G/GCE aimed at the reduction of 200 μM NB in pH 7.0. Inset: the linear relationship between the peak currents and the square root of scan rate. (e) Chronoamperometric response at the GDY/G/GCE in pH 7.0 with different concentrations of NB: 0, 50, 100, and 150 μM. Inset A: the linear relationship between the peak current (I) and $t^{-1/2}$ derived from the chronoamperogram data. Inset B: Dependence of the slope of the straight lines against the NB concentrations. (f) Differential pulse voltammetry curves of 200 μM NB at GDY/G/GCE in 0.1 M PBS with different pH values (5.0, 6.0, 7.0, 8.0, and 9.0). Inset shows the dual plots of peak current and potential versus pH.

3.2. Electrochemical characterization of modified electrodes

By using cyclic voltammetry (CV), the electrochemical behavior of different electrodes was studied (**Fig. 2a**). Since graphene nanosheets can speed up the diffusion of $[Fe(CN)_6]^{3-/4-}$ onto the surface of the electrode, G/GCE exhibits the highest peak current. Nevertheless, owing to the low conductivity of bulk GDY, the peak current significantly drops after modification with GDY (i.e., GDY/GCE). When compared to GDY/GCE, the peak current for GDY/G/GCE shows a significant improvement, proving that graphene can facilitate efficient electron transfer on the electrode surface and increase electrochemical activity.[29-31]

Electrochemical impedance spectroscopy (EIS) is frequently used to study the characteristics of electrode interfaces.[32-34] The Nyquist plots of four modified electrodes are displayed in **Fig. 2b, S2**. The smallest semicircle diameter at high frequency is seen in G/GCE, indicating the lowest charge transfer resistance ($\boldsymbol{R}_{ct}$). The semicircle diameter clearly increases in the case of GDY/GCE, showing an increased $\boldsymbol{R}_{ct}$ of bulk GDY. Interestingly, compared to GDY/GCE, the relevant $\boldsymbol{R}_{ct}$ value drops when GDY is incorporated into graphene. The obvious decrease could be attributed to the addition of conductive graphene, which can reduce the impedance barrier for mass and charge transfer at the electrode surface.

The real electrochemical active surface areas have a great influence on electrochemical behavior.[29, 35] By using CV at various scan rates, the electrochemical surface areas of GDY/G/GCE (**Fig. 2c**) were investigated. It is evident that as the square root of the scan rate increases, the anodic peak current grows linearly. The linear equation can be determined: $I(A)=2.37\times10^{-4}\ v^{1/2}+2.18\times10^{-5}$. As a result, the Randles-Sevcik equation can be used to calculate the electrochemical surface areas:[30, 36]

$$I=(2.69\times10^{5})n^{3/2}ACD^{1/2}v^{1/2} \quad (2)$$

where I is the anodic peak current (A), v is the scan rate (V s^{-1}), A is effective surface area of the working electrode (cm^2), C is the concentration of the electroactive species (mol cm^{-3}), D is the diffusion coefficient of $[Fe(CN)_6]^{3-/4-}$ equal to 7.60×10^{-7} cm^2 s^{-1}, and n is the number of transferred electrons. For comparison, the electrochemical active surface areas of bare GCE, G/GCE, and GDY/GCE were studied under the same conditions (**Fig. S3**). The results show that the electrochemical active surface areas of G/GCE, GDY/GCE, GDY/G/GCE, and bare GCE were 0.109, 0.042, 0.064, and 0.026 cm^2, respectively. In other words, the ultrathin 2D GDY/G heterostructure is expected to enhance electrochemical behavior with high peak currents, smooth electron transfer process, and large electrochemical active surface area. These results confirm that GDY/G/GCE provides a platform for the construction of electrochemical sensors.

3.3. Optimization of experimental parameters

GDY/G heterostructures with different ratio were prepared by changing the amount of HEB (50, 75, 100, 125, and 150 mg). As shown in **Fig. S4**, when HEB was added at 100 mg, the current reached the maximum value. With the amount of HEB increased, the thickness of GDY layer increased and the conductivity of GDY/G heterostructure decreased, because the contribution of graphene to the conductivity of the heterostructure is diminished by the excessively thick GDY layer. The peak current also decreases when HEB content is below 100 mg, which may be due to the discontinuity of the GDY layer loaded on graphene, resulting in fewer adsorption sites. These results indicate that graphene is not only a template to ensure the synthesis of few-layered GDY, but also a cornerstone for the conductivity of GDY/G heterostructure.

The possible influence of scan rate towards NB reduction at GDY/G/GCE were studied by CV (**Fig. 2d**). The reduction peak current increases linearly with the increase of the square root of scan rate (R^2=0.999). This shows that the electrochemical reduction of NB on the modified electrode is driven by a normal diffusion-controlled

process. The diffusion coefficient of the electrochemical process on the electrode surface was studied using the chronoamperometry method (**Fig. 2e**). The diffusion coefficient can be calculated from the Cottrell's equation in the diffusion control process:[37]

$$I=nFAD^{1/2}C\pi^{-1/2}t^{-1/2} \quad (3)$$

where D is the diffusion coefficient ($cm^2\ s^{-1}$) and C is the bulk concentration (mol cm^{-3}). **Inset A of Fig. 2e** shows that $t^{-1/2}$ is linear with the peak current. The concentration of NB is also linear to the slopes in inset A (**inset B of Fig. 2e**). The diffusion coefficient of NB is calculated to 7.033×10^{-6} $cm^2\ s^{-1}$, according to the Cottrell's equation.

When multiple protons are involved in the redox process, the acidity of the detected substance affects the mass transport rate of the electrode surface.[38-40] The effects of pH on the redox current responses and potentials for GDY/G/GCE toward NB were investigated by differential pulse voltammetry (DPV) in PBS at pH values from 5.0 to 9.0 (**Fig. 2f**). The response current increases gradually with pH increasing from 5.0 to 7.0, but then decreases with further the increase of pH value. Hence, pH 7.0 is regarded as the optimum pH for NB detection. In addition, with the increase of pH, the reduction potential shifted negatively, indicating that protons were involved in the charge transfer process.[33] The **inset of Fig. 2f** shows that the reduction potential (Ep) changes linearly with increasing pH. The equation is $E_p(V) = -0.0627\ pH - 0.231$ ($R^2 = 0.998$). The slope of 62.7 mV pH^{-1} is close to the theoretical value of 59 mV pH^{-1}, indicating that the number of protons and electrons transferred during NB reduction is equal.[37, 41]

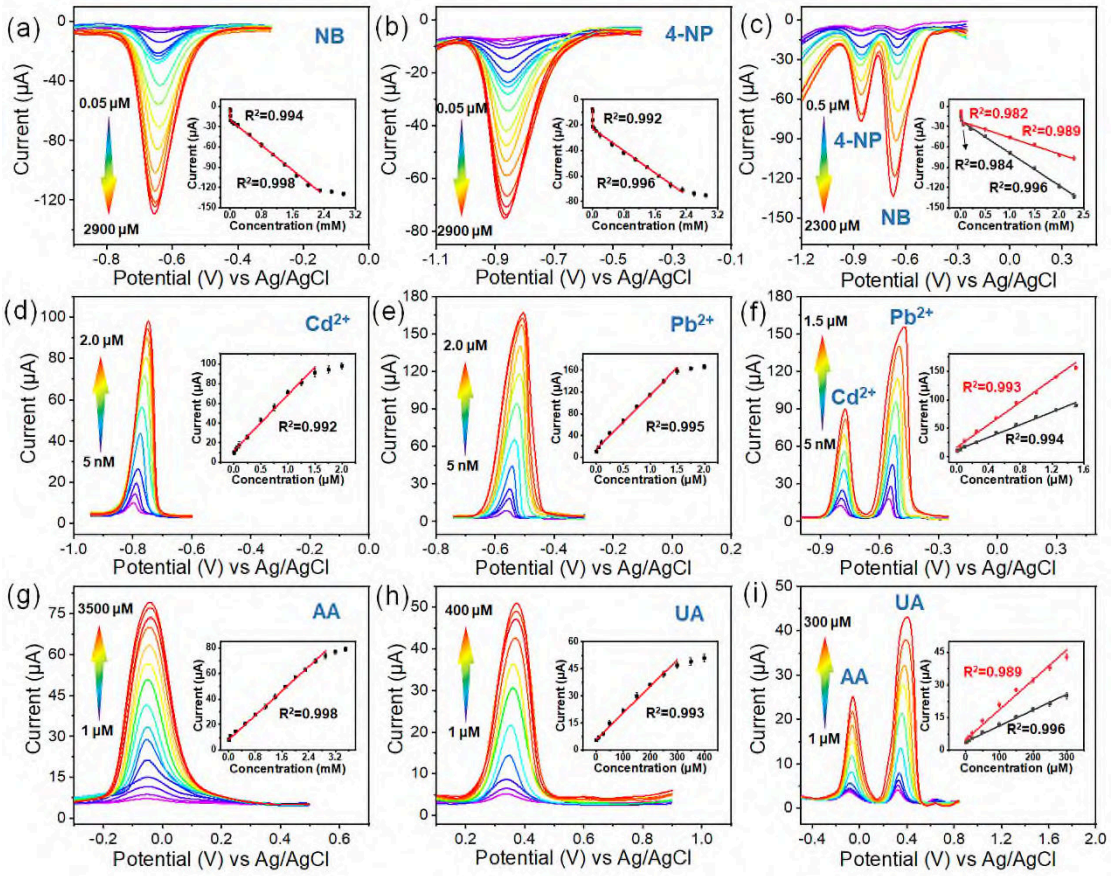


Fig. 3. (a~c) DPV curves of the GDY/G/GCE towards the detection of (a) NB, (b) 4-NP, (c) NB and 4-NP. (d~f) DPASV curves of the GDY/G/GCE towards the detection of (d) Cd^{2+}, (e) Pb^{2+}, (f) Cd^{2+} and Pb^{2+}. (g~i) DPV curves of the hemin/GDY/G/GCE towards the detection of (a) AA, (b) UA, (c) AA and UA. Inset shows linear trend of the peak current versus concentration of corresponding analytes.

3.4. Electrochemical detection of NB on different modified electrodes

The effects of different modified GCE on the electrochemical detection of NB were studied by DPV. As shown in **Fig. S5**, bare GCE displays the lowest peak currents. For GDY and graphene modified GCE, the reduction peak current is significantly enhanced, compared with bare GCE, which can be attributed to the high affinity of graphene and GDY for NB. In addition, the reduction peak current of GDY/GCE is greater than that of G/GCE, which proves that GDY has a stronger affinity for NB than graphene. Specifically, among the investigated four electrodes, GDY/G/GCE possesses the highest reduction peak currents toward NB, revealing the synergistic effect on current signal amplification after GDY payload on the graphene surface. Therefore,

GDY/G/GCE is a promising electrochemical sensing platform for NB detection. Possible reasons for enhanced electrochemical response of GDY/G heterostructures to NB: The template function of graphene enables GDY to grow into a 2D ultrathin structure, which effectively overcomes the shortcoming of the poor conduction of bulk GDY. Few-layered GDY also provides more adsorption sites, which is conducive to the capture of detection signals. Moreover, graphene improves the charge conduction, and finally ensures the efficient redox reaction.

3.5. Electrochemical detection for NB and 4-NP

The feasibility of the GDY/G/GCE electrode for NB and 4-NP detection was examined under optimized conditions by adding different concentrations of NB and 4-NP (**Figs. 3a, 3b**). Notably, as NB and 4-NP concentrations increased, the corresponding reduction peak current also increased linearly. For individual detection, NB and 4-NP showed a two-stage linear relationship in the concentration range of 0.05−2300 μM: y=−1.67x−4.82 (NB, 0.05−10 μM, R^2=0.994), y=−0.046x−20.41 (NB, 10−2300 μM, R^2=0.998), y=−1.49x−7.53 (4-NP, 0.05−10 μM, R^2=0.992) and y=−0.022x−22.73 (4-NP, 10−2300 μM, R^2=0.996). The significant increase in sensitivity to low concentrations may be due to the following factors: (1) abundant catalytic sites at low concentrations are more likely to adsorb NB and 4-NP molecules; (2) these sites are sequestrated due to saturation with NB and 4-NP at higher concentrations, thus reducing sensitivity.[33, 37] The limits of detection for NB and 4-NP are as low as 0.014 μM and 0.016 μM, respectively. Compared with the previously reported modified electrodes for NB and 4-NP detection, GDY/G/GCE exhibits low LOD and wide linear detection range (**Tables S1, S2**). The reasons for outstanding performance may be as follows: (1) The π–π interaction between GDY and benzene ring can facilitate the capture of NB and 4-NP. (2) The evenly distributed pores formed by 18 C atoms in GDY accelerate the transfer of materials and electrons.[41, 42] According to previous reports, this kind of pore structure is helpful in distinguishing substances with similar redox potential.[41] (3) The ultrathin GDY/G heterostructure effectively overcomes the shortcoming of low electron collection efficiency of thick GDY layer,[31] and improves the specific surface area of the material, which provides more adsorption sites. Graphene also improves the conductivity of the electrode material. These characteristics of the GDY/G modified electrode enable the redox reaction to be carried out efficiently.

In addition to the detection of NB and 4-NP individually, the obtained GDY/G/GCE was successfully used for simultaneous electrochemical analysis of NB and 4-NP. **Fig. 3c** shows the DPV response of the mixture of NB and 4-NP under optimal conditions. Evidently, for NB and 4-NP, two separate and well-resolved peaks are seen at 0.64 and 0.86 V, respectively. It is noted that the positions of the reduction peaks when NB and 4-NP coexist are almost unchanged with respect to their individual detection, indicating that the mutual interference between NB and 4-NP is very low. Due to the complete separation of the two peaks, the proposed GDY/G/GCE is anticipated to simultaneously identify NB and 4-NP. As expected, the reduction peak currents of NB and 4-NP also increased linearly with increasing NB and 4-NP concentrations. At the same time, NB and 4-NP have a good linear relationship in the range of 0.5−2300 μM, which can be evaluated as y=−1.33x−7.68 (NB, 0.5−10 μM, R^2=0.984), y=−0.048x−21.71 (NB, 10−2300 μM, R^2=0.996), y=−1.25x−6.79 (4-NP, 0.5−10 μM, R^2=0.982) and y=−0.024x−22.3 (4-NP, 10−2300 μM, R^2=0.989) for NB and 4-NP, respectively. Consequently, LODs for NB and 4-NP are calculated to be 0.018 μM and 0.02 μM, respectively.

3.6. Electrochemical detection for Pb^{2+} and Cd^{2+}

In view of its good response to electrical analysis, differential pulse anodic stripping voltammetry (DPASV) was used to quantitatively determine Pb^{2+} and Cd^{2+} of GDY/G modified GCE. In order to determine the optimal condition of GDY/G/GCE to detect heavy metal ions, the effects of deposition time, pH, and deposition potential on the response current were studied (**Fig. S6**). As shown in **Fig. 3d**, when Cd^{2+} was detected individually, a clear peak was observed at about -0.8 V, which corresponds to the oxidation potential of cadmium. In addition, the relationship between Cd^{2+} concentration and stripping current was linear in the range of 0.005−1.5 μM. The linear equation is defined as: y=56.61x+12.11 (R^2 = 0.992). Therefore, the LOD can be calculated to be 0.31 nM. Similarly, DPASV was used to investigate the response of GDY/G/GCE to Pb^{2+}. **Fig. 3e** shows that there is a sharp peak at the potential of −0.56V, which corresponds to the lead stripping peak. Additionally, In the range of 0.005−1.5 μM, the stripping current increased proportionally with the increase of Pb^{2+} concentration, and the linear relationship was as follows: y=100.42x+14.5 (R^2 = 0.995). Accordingly, the LOD was calculated to be 0.24 nM. Compared with previously reported modified electrodes for Pb^{2+} and Cd^{2+} detection, GDY/G/GCE has a lower LOD and a wide linear range (**Tables S3, S4**). Compared with the π–π interaction of

organic pollutant detection, the excellent performance of heavy metal ions detection can be attributed to: (1) the acetylenic linkages of GDY are rich in π-electrons, making the surface of GDY more negative, which facilitates the approach of metal cations.[21, 43] (2) The unique pore structure of GDY allows heavy metal ions to be embedded, providing an ideal adsorption location.[26, 31]

As shown in **Fig. 3f**, GDY/G/GCE also implements simultaneous detection of Pb^{2+} and Cd^{2+}. In the concentration range of 0.005−1.5 μM, the current response of GDY/G/GCE rises with the increasing of Pb^{2+} and Cd^{2+} concentrations. The LODs can be calculated as 0.25 (Pb^{2+}) and 0.32 (Cd^{2+}) nM, respectively. Since the two peaks are completely separated and each shows a good linear relationship, the proposed GDY/G/GCE is likely to simultaneously identify Pb^{2+} and Cd^{2+}.

3.7. Electrochemical detection for AA and UA

Hemin as a key enzyme catalytic motif was immobilized on GDY/G via π–π interaction, details of the synthesis, characterization, and optimization of hemin/GDY/G are provided in supporting information (**Figs. S7~S9**). Electrode modified with hemin/GDY/G was successfully used for AA and UA detection. **Fig. 3g** reveals the DPV curves of different AA concentrations. As the concentration of AA increases from 1−2900 μM, the current response of the oxidation peak increases linearly at the potential of -0.052 V. The linear equation is described as: y=0.024x+8.23 (R^2=0.998). The corresponding LOD is calculated to be 2.73 μM. Similarly, **Fig. 3h** displays the peak current response increase linearly at the potential of 0.336 V with the UA concentration increasing from 1 to 300 μM. The linear equation is y=0.14x+6.01 (R^2=0.993). Accordingly, the LOD can be calculated to be 0.081 μM. To demonstrate the good performance of hemin/GDY/G/GCE, the linear range and LOD were compared with biosensors previously reported for AA and UA detection (**Tables S5, S6**). It can be seen that the proposed biosensor has a low detection limit and a wide linear range.

For the simultaneous detection of AA and UA, **Fig. 3i** shows the oxidation reaction of a mixture of AA and UA on hemin/GDY/G/GCE. The two well-defined voltammetric peaks observed correspond to the oxidation of AA and UA, respectively, and the peak currents increase with increasing concentrations of AA and UA. The results reveal that the hemin/GDY/G modified sensor can accomplish the simultaneous detection of AA and UA.

3.8. Selectivity, reproducibility and stability of sensors

The stability and reproducibility are important factors of electrochemical sensors. GDY/G/GCE showed an excellent stability, and retained 98.9%, 98.6%, 97.6% and 96.6% of initial response for NB, 4-NP, Pb^{2+} and Cd^{2+} after 30 days, respectively (**Figs. S10a, S10b**). Hemin/GDY/G/GCE retained 97.4% and 98.4% of initial response for AA and UA after 30 days (**Fig. S10c**). Moreover, the stability of after different temperature (-20°C, 70°C) treatment was tested (**Fig. S11**). It retained above 97% of the response at 25°C for NB, 4-NP, Pb^{2+}, Cd^{2+}, AA and UA, this is attributed to the high physical and chemical stability of carbon material, i.e. GDY and graphene.[44, 45] Furthermore, the UV-Vis spectra of hemin/GDY/G were compared (**Fig. S12**). It was found that the modified electrode had the same molecular structure before and after continuous detection, indicating that hemin loaded on GDY/G heterostructure had excellent stability.

Besides, to evaluate the repeatability of the proposed sensor, 10 experiments were repeated at the same electrode. As shown in **Figs. 4a, 4b** the GDY/G/GCE had satisfactory reproducibility (NB, RSD = 0.7 %; 4-NP, RSD = 1.50 %; Pb^{2+}, RSD = 1.48 %; Cd^{2+}, RSD = 2.09 %). At the same time, hemin/GDY/G/GCE also shows excellent reproducibility (AA, RSD = 1.48 %; UA, RSD = 1.06 %) (**Fig. 4c**).

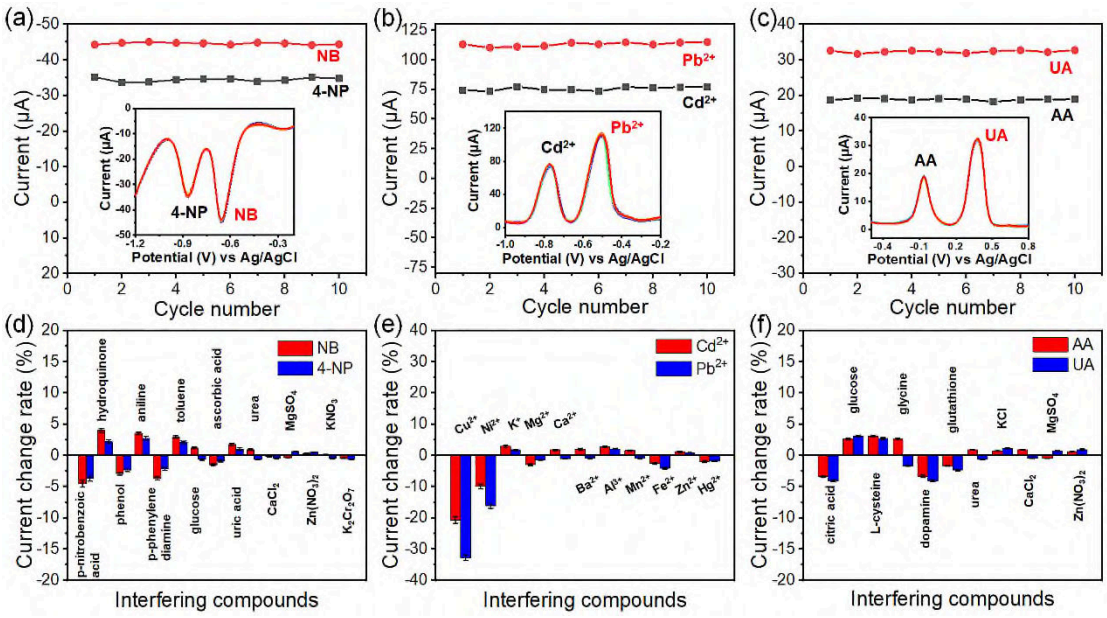


Fig. 4. (a, b) The reproducibility of the GDY/G/GCE. (a) 500 μM NB and 4-NP in pH 7.0, (b) 1 μM Cd^{2+} and Pb^{2+} in pH 5.0. (c) The reproducibility of the hemin/GDY/G/GCE towards the detection of 200 μM AA and UA in pH 7.0. (d, e) The

selectivity of GDY/G/GCE towards the detection of (d) NB and 4-NP, and (e) Pb^{2+} and Cd^{2+}. (f) The selectivity of hemin/GDY/G/GCE towards the detection of AA and UA, each corresponding to additions of 5-fold of different interferents.

The selectivity of GDY/G/GCE was evaluated by adding 5-fold molar amount of interferents to 200 μM NB and 4-NP solution (**Fig. 4d**). It can be seen that the interference of common metal ions and biological species on the detection of NB and 4-NP is negligible (<2%), while benzene derivatives and phenolic compounds have only slight influence in NB and 4-NP detection (<5%). These results indicate that the modified electrode can selectively detect NB and 4-NP even in the presence of excessive amounts of these potential interfering substances. The selectivity of GDY/G/GCE for Cd^{2+} and Pb^{2+} detection was also evaluated. 5-Fold molar amount of common metal ions were added to 1 μM Pb^{2+} and Cd^{2+} mixture solution simultaneous detection to investigate the change of response current. As can be seen from **Fig. 4e**, except Ni^{2+} and Cu^{2+}, the relative signal changes of other interfering ions are within the tolerance rate of ±5%, which means that the interference of non-target ions is small, demonstrating that GDY/G/GCE has high selectivity for Pb^{2+} and Cd^{2+} in the existence of other interfering ions. The interference of Cu^{2+} and Ni^{2+} was further studied, which may be due to chemisorption interaction between GDY and Cu^{2+}/Ni^{2+} and the Cu-Pb interaction.[46-49] However, potassium ferrocyanide as masking agent can reduce the interference of Cu^{2+} and Ni^{2+} (**Figs. S13a, S13b**).[21] Furthermore, hemin/GDY/G/GCE also showed excellent selectivity for AA and UA detection, with only slight interference (<5%) from several typical interferers, as shown in **Fig. 4f.**

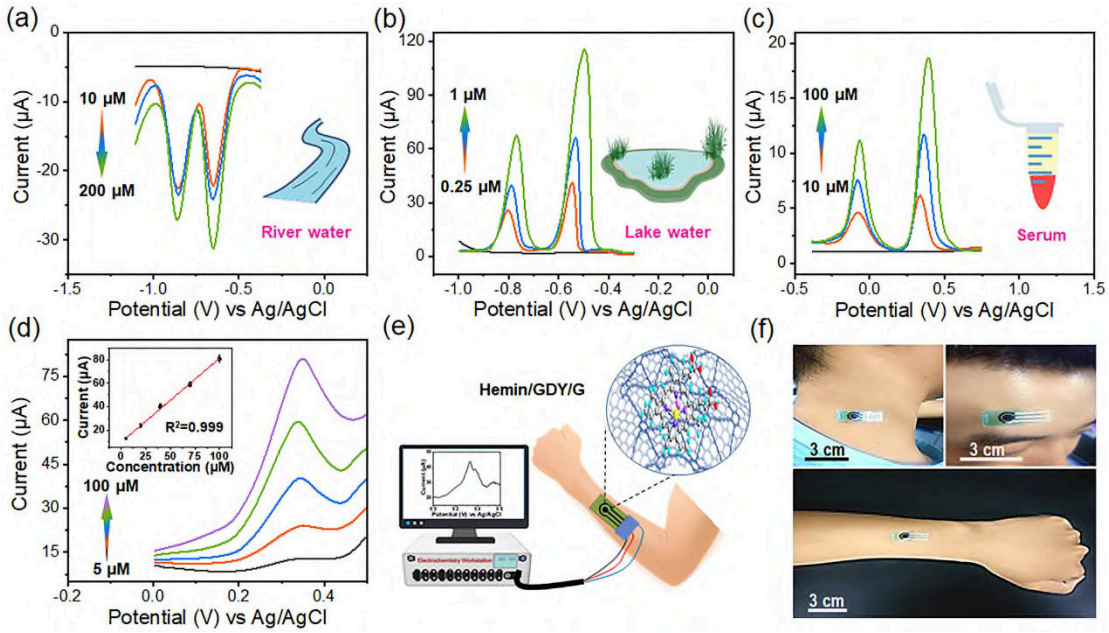


Fig. 5. (a, b) The real sample analysis of GDY/G/GCE. (a) River water with different amounts of NB and 4-NP in pH 7.0. (b) Lake water with different amounts of Cd^{2+} and Pb^{2+} in pH 5.0. (c) The real sample analysis of hemin/GDY/G/GCE in serum with different amounts of AA and UA in pH 7.0. (d) DPV curves of different UA (5, 20, 40, 70, and 100 μM) concentrations at hemin/GDY/G modified screen-printed electrode. Inset shows the linear relationship between peak current and UA concentration. (e) Schematic diagram of the flexible and wearable sensor for UA sensing in human sweat. (f) Demonstration photos of the wearable biosensors attached on different parts of the body for monitoring.

3.9. Real sample detection

To further evaluate the feasibility of the proposed sensor, NB and 4-NP in river water were detected using modified electrode by adding different concentrations of NB and 4-NP (10 μM, 50 μM and 200 μM), and three parallel measurements were made at each concentration level (**Fig. 5a**). As shown in **Table S7**, the detection of NB and 4-NP by GDY/G/GCE has excellent recoveries, and the RSD is less than 4.48%. In addition, samples were analyzed by high performance liquid chromatography (HPLC) to verify the performance of the proposed sensor (**Table S8**). It can be seen that there is no significant difference between the two methods, indicating the reliability of the developed sensor. Similarly, the feasibility of testing for Pb^{2+} and Cd^{2+} in lake water (**Fig. 5b**) and AA and UA in serum (**Fig. 5c**) was evaluated. Compared with inductively

coupled plasma mass spectrometry (ICP-MS), HPLC and Colorimetric kit, the proposed sensor exhibits good recoveries and low RSDs .

Furthermore, hemin/GDY/G was modified on a commercial screen-printed electrode to monitor UA in human sweat to verify the feasibility of our electrochemical sensing platform as a wearable biosensor. As shown in **Fig. 5d**, 5 UA standard solutions were measured, which is in a good linear correlation. **Fig. 5e** is a schematic diagram of UA detection in human sweat. The sensor can be attached to different parts of the skin well to achieve the purpose of wearable detection (**Fig. 5f**). Three samples were measured by using the modified screen-printed electrodes, sweat was collected from different volunteers (24, 40, and 60 years). For comparison, UA concentration was determined using commercial colorimetric assay kit. Since UA concentration is proportional to absorbance, the amount of UA in sweat was calculated from the standard curve (**Fig. S14a**). As shown in **Fig. S14b**, the results of the two analytical methods have good correlation, which showing the sensing platform holds great potential in wearable biosensing.

4. CONCLUSION

In summary, GDY/G 2D heterostructure was synthesized and employed for electrochemical detection of multiple targets. Compared with GDY, GDY/G shows lower electrochemical impedance, and higher electrochemical active surface area, which are conducive to the diffusion of substances and electron transfer. GDY/G was used as a new electrode material in the electrochemical sensor, which shows high sensitivity for heavy metal ions (Pb^{2+}, Cd^{2+}) and toxic molecules (NB, 4-NP) due to the d–π and π–π interaction, respectively. Moreover, hemin as a key enzyme catalytic motif was immobilized on GDY/G via π–π interaction, the sandwich structure of hemin/GDY/G was successfully utilized for AA and UA detection. Finally, the prepared electrode showed satisfactory recovery and RSD in real sample analysis, including waster and biological samples. And the flexible and wearable UA sensor also demonstrate the promising for the detection of UA in human sweat. This study demonstrates that GDY/G heterostructure can be used as a powerful electrochemical sensing platform for the detection of a wide range of environmental pollutants and medical diagnosis.

ASSOCIATED CONTENT

Supporting Information.

The Supporting Information is available free of charge on the ACS Publications website.

Additional detailed experimental procedures, SEM of GDY, EIS of bare GCE, CV and DPV of modified electrode, optimization of HEB content, optimization of heavy metal ion detection conditions, UV-Vis and EDS characterization of hemin and hemin/GDY/G, hemin load ratio optimization, stability experiment, experiments with masking agents, standard curves of the UA assay kit, comparison of uric acid colorimetric assay and electrochemical method, comparison of linear range and LOD with literature, real sample analysis (PDF)

AUTHOR INFORMATION

Corresponding Authors

Lina Wang – *College of Environment and Safety Engineering, Qingdao University of Science and Technology, Qingdao, Shandong 266042, China;* orcid.org/0000-0001-8633-4674; E-mail: linawang@qust.edu.cn

Zhiling Zhu – *College of Materials Science and Engineering, Qingdao University of Science and Technology, Qingdao, Shandong 266042, China;* orcid.org/0000-0003-3878-0391; E-mail: zlzhu@qust.edu.cn

Ning Sui – *College of Materials Science and Engineering, Qingdao University of Science and Technology, Qingdao, Shandong 266042, China;* orcid.org/0000-0002-0543-8701; E-mail: suining@qust.edu.cn

Authors

Xiuchao Sun – *College of Materials Science and Engineering, Qingdao University of Science and Technology, Qingdao, Shandong 266042, China*

Menglu Duan – *College of Materials Science and Engineering, Qingdao University of Science and Technology, Qingdao, Shandong 266042, China*

Rongteng Li – *College of Materials Science and Engineering, Qingdao University of Science and Technology, Qingdao, Shandong 266042, China*

Yuan Meng – *College of Materials Science and Engineering, Qingdao University of Science and Technology, Qingdao, Shandong 266042, China*

Qiang Bai – *College of Materials Science and Engineering, Qingdao University of Science and Technology, Qingdao, Shandong 266042, China*

Manhong Liu – *College of Materials Science and Engineering, Qingdao University of Science and Technology, Qingdao, Shandong 266042, China*

Zhugen Yang – *School of Water, Energy and Environment, Cranfield University, Milton Keynes, MK43 0AL, United Kingdom*

Notes

The authors declare no competing financial interest.

Acknowledgements

The authors acknowledge the National Natural Science Foundation of China (31800800, 21501106) and Natural Science Foundation of Shandong Province China (ZR2019BC101, ZR2020MB026, ZR202103010467). ZY thanks UK NERC Fellowship grant (NE/R013349/2).

References

1. Hu, W.; Chang, Y.; Huang, J.; Chai, Y.; Yuan, R., Tetrahedral DNA Nanostructure with Multiple Target-Recognition Domains for Ultrasensitive Electrochemical Detection of Mucin 1. *Analytical Chemistry* **2022,** *94* (18), 6860-6865.
2. Banga, I.; Paul, A.; Muthukumar, S.; Prasad, S., ZENose (ZIF-Based Electrochemical Nose) Platform for Noninvasive Ammonia Detection. *ACS Applied Materials & Interfaces* **2021,** *13* (14), 16155-16165.
3. Wang, C.; Li, J.; Kang, M.; Huang, X.; Liu, Y.; Zhou, N.; Zhang, Z., Nanodiamonds and Hydrogen-Substituted Graphdiyne Heteronanostructure for the Sensitive Impedimetric Aptasensing of Myocardial Infarction and Cardiac Troponin I. *Analytica Chimica Acta* **2021,** *1141*, 110-119.
4. Wu, L.; Gao, J.; Lu, X.; Huang, C.; Dhanjai; Chen, J., Graphdiyne: A New Promising Member of 2D All-Carbon Nanomaterial as Robust Electrochemical Enzyme Biosensor Platform. *Carbon* **2020,** *156*, 568-575.
5. Kokulnathan, T.; Wang, T.-J.; Ashok Kumar, E.; Ahmed, F., Construction of Nickel Cobalt-Layered Double Hydroxide/Functionalized–Halloysite Nanotubes

Composite for Electrochemical Detection of Organophosphate Insecticide. *Chemical Engineering Journal* **2022,** *433*, 133639.

6. Lin, M.; Wan, H.; Zhang, J.; Wang, Q.; Hu, X.; Xia, F., Electrochemical DNA Sensors Based on MoS_2-AuNPs for Polynucleotide Kinase Activity and Inhibition Assay. *ACS Applied Materials & Interfaces* **2020,** *12* (41), 45814-45821.

7. Suhito, I. R.; Kim, J. W.; Koo, K.-M.; Nam, S. A.; Kim, Y. K.; Kim, T.-H., In Situ Detection of Kidney Organoid Generation From Stem Cells Using a Simple Electrochemical Method. *Advanced Science* **2022,** *n/a* (n/a), 2200074.

8. Wu, N.; Jiao, L.; Song, S.; Wei, X.; Cai, X.; Huang, J.; Sha, M.; Gu, W.; Song, W.; Zhu, C., Tuning the Ratio of Pt(0)/Pt(II) in Well-Defined Pt Clusters Enables Enhanced Electrocatalytic Reduction/Oxidation of Hydrogen Peroxide for Sensitive Biosensing. *Analytical Chemistry* **2021,** *93* (48), 15982-15989.

9. Fu, C.; Yi, D.; Deng, C.; Wang, X.; Zhang, W.; Tang, Y.; Caruso, F.; Wang, Y., A Partially Graphitic Mesoporous Carbon Membrane with Three-Dimensionally Networked Nanotunnels for Ultrasensitive Electrochemical Detection. *Chemistry of Materials* **2017,** *29* (12), 5286-5293.

10. Chen, Y.; Liu, B.; Chen, Z.; Zuo, X., Innovative Electrochemical Sensor Using TiO_2 Nanomaterials to Detect Phosphopeptides. *Analytical Chemistry* **2021,** *93* (30), 10635-10643.

11. Dau, T. N. N.; Vu, V. H.; Cao, T. T.; Nguyen, V. C.; Ly, C. T.; Tran, D. L.; Pham, T. T. N.; Loc, N. T.; Piro, B.; Vu, T. T., In-Situ Electrochemically Deposited Fe_3O_4 Nanoparticles onto Graphene Nanosheets as Amperometric Amplifier for Electrochemical Biosensing Applications. *Sensors and Actuators B: Chemical* **2019,** *283*, 52-60.

12. Huang, L.; Chen, H.; Diao, D., Manufacturing High-Density Graphene Edges with Electrochemical Etching for Sensing Aminophenol. *Analytica Chimica Acta* **2022,** *1198*, 339527.

13. Prakash, J.; Dey, A.; Uppal, S.; Alexander, R.; Kaushal, A.; Misra, H. S.; Dasgupta, K., Label-Free Rapid Electrochemical Detection of DNA Hybridization Using Ultrasensitive Standalone CNT Aerogel Biosensor. *Biosensors and Bioelectronics* **2021,** *191*, 113480.

14. Bi, Y.; Hei, Y.; Wang, N.; Liu, J.; Ma, C.-B., Synthesis of a Clustered Carbon Aerogel Interconnected by Carbon Balls from the Biomass of Taros for Construction of a Multi-Functional Electrochemical Sensor. *Analytica Chimica Acta* **2021,** *1164*, 338514.

15. Guo, S.; Yan, H.; Wu, F.; Zhao, L.; Yu, P.; Liu, H.; Li, Y.; Mao, L., Graphdiyne as Electrode Material: Tuning Electronic State and Surface Chemistry for Improved Electrode Reactivity. *Analytical Chemistry* **2017,** *89* (23), 13008-13015.
16. Zhou, J.; Li, J.; Liu, Z.; Zhang, J., Exploring Approaches for the Synthesis of Few-Layered Graphdiyne. *Advanced Materials* **2019,** *31* (42), 1803758.
17. Bai, Q.; Luo, H.; Yi, X.; Shi, S.; Wang, L.; Liu, M.; Du, F.; Yang, Z.; Sui, N., Nitrogen-Doped Graphdiyne Quantum-Dots as an Optical-Electrochemical Sensor for Sensitive Detection of Dopamine. *Microchemical Journal* **2022,** *179*, 107521.
18. Cui, J.; Liu, J.; Wang, C.; Rong, F.; He, L.; Song, Y.; Zhang, Z.; Fang, S., Efficient Electrocatalytic Water Oxidation by Using the Hierarchical 1D/2D Structural Nanohybrid of CoCu-Based Zeolitic Imidazolate Framework Nanosheets and Graphdiyne Nanowires. *Electrochimica Acta* **2020,** *334*, 135577.
19. Chauhan, D.; Kumar, Y.; Chandra, R.; Kumar, S., 2D Transparent Few-Layered Hydrogen Substituted Graphdiyne Nano-Interface for Unprecedented Ultralow ANXA2 Cancer Biomarker Detection. *Biosensors and Bioelectronics* **2022,** *213*, 114433.
20. Hou, Y.-Y.; Xu, J.; Wang, F.-T.; Dong, Z.; Tan, X.; Huang, K.-J.; Li, J.-Q.; Zuo, C.-Y.; Zhang, S.-Q., Construction of an Integrated Device of a Self-Powered Biosensor and Matching Capacitor Based on Graphdiyne and Multiple Signal Amplification: Ultrasensitive Method for MicroRNA Detection. *Analytical Chemistry* **2021,** *93* (46), 15225-15230.
21. Li, Y.; Huang, H.; Cui, R.; Wang, D.; Yin, Z.; Wang, D.; Zheng, L.; Zhang, J.; Zhao, Y.; Yuan, H.; Dong, J.; Guo, X.; Sun, B., Electrochemical Sensor Based on Graphdiyne is Effectively Used to Determine Cd^{2+} and Pb^{2+} in Water. *Sensors and Actuators B: Chemical* **2021,** *332*, 129519.
22. Niu, K.; Gao, J.; Wu, L.; Lu, X.; Chen, J., Nitrogen-Doped Graphdiyne as a Robust Electrochemical Biosensing Platform for Ultrasensitive Detection of Environmental Pollutants. *Analytical Chemistry* **2021,** *93* (24), 8656-8662.
23. Shi, M.; Sun, X.; Bai, Q.; Zhang, Y.; Yu, S.; Liu, M.; Wang, L.; Yu, W. W.; Sui, N., Graphdiyne/Graphene Heterostructure Supported NiFe Layered Double Hydroxides for Oxygen Evolution Reaction. *Colloids and Surfaces A: Physicochemical and Engineering Aspects* **2022,** *637*, 128217.
24. Gao, X.; Zhu, Y.; Yi, D.; Zhou, J.; Zhang, S.; Yin, C.; Ding, F.; Zhang, S.; Yi, X.; Wang, J.; Tong, L.; Han, Y.; Liu, Z.; Zhang, J., Ultrathin

Graphdiyne Film on Graphene Through Solution-Phase Van Der Waals Epitaxy. *Science Advances* **2018,** *4*, eaat6378.

25. Li, J.; Yi, Y.; Zuo, X.; Hu, B.; Xiao, Z.; Lian, R.; Kong, Y.; Tong, L.; Shao, R.; Sun, J.; Zhang, J., Graphdiyne/Graphene/Graphdiyne Sandwiched Carbonaceous Anode for Potassium-Ion Batteries. *ACS Nano* **2022,** *16* (2), 3163-3172.

26. Li, J.; Zhong, L.; Tong, L.; Yu, Y.; Liu, Q.; Zhang, S.; Yin, C.; Qiao, L.; Li, S.; Si, R.; Zhang, J., Atomic Pd on Graphdiyne/Graphene Heterostructure as Efficient Catalyst for Aromatic Nitroreduction. *Advanced Functional Materials* **2019,** *29* (43), 1905423.

27. Gu, H.; Zhong, L.; Shi, G.; Li, J.; Yu, K.; Li, J.; Zhang, S.; Zhu, C.; Chen, S.; Yang, C.; Kong, Y.; Chen, C.; Li, S.; Zhang, J.; Zhang, L., Graphdiyne/Graphene Heterostructure: A Universal 2D Scaffold Anchoring Monodispersed Transition-Metal Phthalocyanines for Selective and Durable CO_2 Electroreduction. *Journal of the American Chemical Society* **2021,** *143* (23), 8679-8688.

28. Zhang, Q.; Bai, Q.; Cai, E.; Hao, L.; Wang, M.; Zhang, S.; Zhao, Q.; Teng, L.; Sui, N.; Du, F.; Wang, X., Nonlinear Optical Properties of Graphdiyne/Graphene Van Der Waals Heterostructure for Laser Modulations. *Results in Physics* **2022,** *38*, 105654.

29. Wang, J.; Yu, P.; Kan, K.; Lv, H.; Liu, Z.; Sun, B.; Bai, X.; Chen, J.; Zhang, Y.; Shi, K., Efficient Ultra-Trace Electrochemical Detection of Cd^{2+}, Pb^{2+} and Hg^{2+} Based on Hierarchical Porous S-Doped C_3N_4 Tube Bundles/Graphene Nanosheets Composite. *Chemical Engineering Journal* **2021,** *420*, 130317.

30. Ma, Y.; Wang, Y.; Xie, D.; Gu, Y.; Zhu, X.; Zhang, H.; Wang, G.; Zhang, Y.; Zhao, H., Hierarchical MgFe-Layered Double Hydroxide Microsphere/Graphene Composite for Simultaneous Electrochemical Determination of Trace Pb(II) and Cd(II). *Chemical Engineering Journal* **2018,** *347*, 953-962.

31. Lv, Y.; Wu, X.; Lin, H.; Li, J.; Zhang, H.; Guo, J.; Jia, D.; Zhang, H., A Novel Carbon Support: Few-Layered Graphdiyne-Decorated Carbon Nanotubes Capture Metal Clusters as Effective Metal-Supported Catalysts. *Small* **2021,** *17* (12), 2006442.

32. Biswas, S.; Chen, Y.; Xie, Y.; Sun, X.; Wang, Y., Ultrasmall Au(0) Inserted Hollow PCN-222 MOF for the High-Sensitive Detection of Estradiol. *Analytical Chemistry* **2020,** *92* (6), 4566-4572.

33. Chen, Y.; Sun, X.; Biswas, S.; Xie, Y.; Wang, Y.; Hu, X., Integrating Polythiophene Derivates to PCN-222(Fe) for Electrocatalytic Sensing of L-Dopa. *Biosensors and Bioelectronics* **2019,** *141*, 111470.

34. Wang, Y.; Wang, L.; Chen, H.; Hu, X.; Ma, S., Fabrication of Highly Sensitive and Stable Hydroxylamine Electrochemical Sensor Based on Gold Nanoparticles and Metal–Metalloporphyrin Framework Modified Electrode. *ACS Applied Materials & Interfaces* **2016,** *8* (28), 18173-18181.

35. Wang, Y.; Wang, L.; Huang, W.; Zhang, T.; Hu, X.; Perman, J. A.; Ma, S., A Metal–Organic Framework and Conducting Polymer Based Electrochemical Sensor for High Performance Cadmium Ion Detection. *Journal of Materials Chemistry A* **2017,** *5* (18), 8385-8393.

36. Yang, J.; Gunasekaran, S., Electrochemically Reduced Graphene Oxide Sheets for Use in High Performance Supercapacitors. *Carbon* **2013,** *51*, 36-44.

37. Zhou, Z.; Mukherjee, S.; Hou, S.; Li, W.; Elsner, M.; Fischer, R. A., Porphyrinic MOF Film for Multifaceted Electrochemical Sensing. *Angewandte Chemie International Edition* **2021,** *60* (37), 20551-20557.

38. Zhu, W.; Gao, J.; Song, H.; Lin, X.; Zhang, S., Nature of the Synergistic Effect of N and S Co-Doped Graphene for the Enhanced Simultaneous Determination of Toxic Pollutants. *ACS Applied Materials & Interfaces* **2019,** *11* (47), 44545-44555.

39. Gao, J.; Liu, M.; Song, H.; Zhang, S.; Qian, Y.; Li, A., Highly-Sensitive Electrocatalytic Determination for Toxic Phenols Based on Coupled cMWCNT/Cyclodextrin Edge-Functionalized Graphene Composite. *Journal of Hazardous Materials* **2016,** *318*, 99-108.

40. Gao, J.; Fang, J.; Ju, X.; Zhu, W.; Lin, X.; Zhang, S.; Ma, C.; Song, H., Hierarchical Self-Assembly of Cyclodextrin and Dimethylamino-Substituted Arylene–Ethynylene on N-doped Graphene for Synergistically Enhanced Electrochemical Sensing of Dihydroxybenzene Isomers. *ACS Applied Materials & Interfaces* **2017,** *9* (44), 38802-38813.

41. Zhang, Y.; Xie, Q.; Xia, Z.; Gui, G.; Deng, F., Graphdiyne Oxides as New Modifier for the Simultaneous Electrochemical Detection of Phenolic Compounds. *Journal of Electroanalytical Chemistry* **2020,** *863*, 114058.

42. Nan, D.; Huang, Z.-H.; Lv, R.; Yang, L.; Wang, J.-G.; Shen, W.; Lin, Y.; Yu, X.; Ye, L.; Sun, H.; Kang, F., Nitrogen-Enriched Electrospun Porous Carbon Nanofiber Networks as High-Performance Free-Standing Electrode Materials. *Journal of Materials Chemistry A* **2014,** *2* (46), 19678-19684.

43. Guo, X.; Li, Y.; Huang, H.; Wang, D.; Cui, R.; Li, J.; Zhao, Y.; Wang, D.; Yuan, H.; Dong, J.; Sun, B., Triazine-Graphdiyne with Well-Defined Two Kinds of Active Sites for Simultaneous Detection of Pb^{2+} and Cd^{2+}. *Journal of Environmental Chemical Engineering* **2022,** *10* (2), 107159.

44. Poletti, F.; Scidà, A.; Zanfrognini, B.; Kovtun, A.; Parkula, V.; Favaretto, L.; Melucci, M.; Palermo, V.; Treossi, E.; Zanardi, C., Graphene-Paper-Based Electrodes on Plastic and Textile Supports as New Platforms for Amperometric Biosensing. *Advanced Functional Materials* **2022,** *32* (7), 2107941.

45. Niu, K.; Zuo, Z.; Lu, X.; Zou, L.; Chen, J., Ultrathin Graphdiyne Nanosheets Confining Cu Quantum Dots as Robust Electrocatalyst for Biosensing Featuring Remarkably Enhanced Activity and Stability. *Biosensors and Bioelectronics* **2022,** *205*, 114111.

46. Zhai, Z.; Huang, N.; Zhuang, H.; Liu, L.; Yang, B.; Wang, C.; Gai, Z.; Guo, F.; Li, Z.; Jiang, X., A Diamond/Graphite Nanoplatelets Electrode for Anodic Stripping Voltammetric Trace Determination of Zn(II), Cd(II), Pb(II) and Cu(II). *Applied Surface Science* **2018,** *457*, 1192-1201.

47. Mashhadzadeh, A. H.; Vahedi, A. M.; Ardjmand, M.; Ahangari, M. G., Investigation of Heavy Metal Atoms Adsorption onto Graphene and Graphdiyne Surface: A Density Functional Theory Study. *Superlattices and Microstructures* **2016,** *100*, 1094-1102.

48. He, J.; Wang, N.; Yang, Z.; Shen, X.; Wang, K.; Huang, C.; Yi, Y.; Tu, Z.; Li, Y., Fluoride Graphdiyne as a Free-Standing Electrode Displaying Ultra-Stable and Extraordinary High Li Storage Performance. *Energy & Environmental Science* **2018,** *11* (10), 2893-2903.

49. Sun, M.; Wu, T.; Xue, Y.; Dougherty, A. W.; Huang, B.; Li, Y.; Yan, C.-H., Mapping of Atomic Catalyst on Graphdiyne. *Nano Energy* **2019,** *62*, 754-763.



https://dspace.org/

Ultrathin graphdiyne/graphene heterostructure as a robust electrochemical sensing platform

Sun, Xiuchao; Duan, Menglu; Li, Rongteng; Meng, Yuan; Bai, Qiang ...

2022-09-19
American Chemical Society
https://doi.org/10.1021/acs.analchem.2c03387
Sun X, Duan M, Li R, et al., (2022) Ultrathin graphdiyne/graphene heterostructure as a robust electrochemical sensing platform. Analytical Chemistry, Volume 94, Issue 39, September 2022, pp. 13598-13606

Downloaded from a DSpace repository. https://dspace.org/